Viability of Mouse Retinal Explant Cultures Assessed by Preservation of Functionality and Morphology

Virpi Alarautalahti,[1] Symantas Ragauskas,[2] Jenni J. Hakkarainen,[2] Hannele Uusitalo-Järvinen,[1,3] Hannu Uusitalo,[1,3] Jari Hyttinen,[1] Giedrius Kalesnykas,[2] and Soile Nymark[1]

[1]Faculty of Medicine and Health Technology, Tampere University, Tampere, Finland
[2]Experimentica Ltd., Kuopio, Finland
[3]Tays Eye Centre, Tampere University Hospital, Tampere, Finland

Correspondence: Soile Nymark, Faculty of Medicine and Health Technology, Tampere University, Arvo Ylpön Katu 34, Tampere 33520, Finland; soile.nymark@tuni.fi.

Submitted: June 29, 2018
Accepted: March 4, 2019

Citation: Alarautalahti V, Ragauskas S, Hakkarainen JJ, et al. Viability of mouse retinal explant cultures assessed by preservation of functionality and morphology. *Invest Ophthalmol Vis Sci*. 2019;60:1914–1927. https://doi.org/10.1167/iovs.18-25156

Purpose. Retinal explant cultures provide simplified systems where the functions of the retina and the effects of ocular therapies can be studied in an isolated environment. The purpose of this study was to provide insight into long-term preservation of retinal tissue in culture conditions, enable a deeper understanding of the interdependence of retinal morphology and function, and ensure the reliability of the explant technique for prolonged experiments.

Methods. Retinal explants from adult mice were cultured as organotypic culture at the air-medium interface for 14 days in vitro (DIV). Retinal functionality was assessed by multielectrode array technique and morphology by immunohistochemical methods at several time points during culture.

Results. Retinal explants retained viability for 14 DIV, although with diminishing neuronal activity, progressing neuronal loss, and increasing reactive gliosis. We recorded spontaneous retinal ganglion cell (RGC) activity up to 14 DIV with temporally changing distribution of RGC firing rates. Light responsiveness was measurable from RGCs for 7 DIV and from photoreceptors for 2 DIV. Apoptotic cells were detected beginning at 3 DIV with their density peaking at 7 DIV. The number of RGCs gradually decreased by 70% during 14 DIV. The change was accompanied by the loss of RGC functionality, resulting in 84% loss of electrically active RGCs.

Conclusions. Retinal explants provide a valuable tool for studies of retinal functions and development of ocular therapies. However, critical for long-term use, retinal functionality was lost before structural loss, emphasizing a need for both functional and morphologic readouts to determine the overall state of the cultured retina.

Keywords: retina, explant culture, electrophysiology

In vitro models are valuable tools for the development of therapies and pathogenic investigation of various diseases complementing in vivo studies.[1] These models fill the gap between in vivo studies that are expensive and time consuming, with complexities arising from systemic effects and inaccessibility of target tissue, and cell cultures that are less expensive and rapid, but limited in their ability to mimic the in vivo situation. Retinal explant culture, an in vitro model for retinal studies, provides a simplified system for investigating the functioning of the retina and the effects of different therapeutic approaches in an isolated environment.[2] An emerging retinal culture model is an organotypic explant culture in which a small piece of retina is cultured on an organotypic filter.[3–13] In organotypic systems, many of the retinal cell types and their morphologic interactions are maintained intact.[4] Yet, the extent to which retinal cells retain their viability in culture conditions has not been fully evaluated.

Organotypic retinal explant cultures have been used to study retinal development,[14–16] retinal diseases and injuries,[17–26] drug screening,[3,27–33] and retinal stem cell therapies.[8,34,35] The culture systems also have high potential outside these fields, and they could be beneficial for completely new fields, including prion research and, specifically, prion organotypic slice culture assays.[36] Rodent retinae are most commonly used in explant cultures due to their flexibility in gene manipulation.[35,37] In addition, human organotypic retinal culture models have recently been developed and characterized[5,11,18] (Szabo A, et al. *IOVS* 2018;59:ARVO E-Abstract 4021). The organotypic cultures have high potential as tools for testing pharmacologic compounds since a serum-free and chemically defined in vitro environment allows accurate and reproducible manipulation of the experimental conditions. For evaluating the retinal responses to these manipulations, knowledge regarding the preservation of retinal functionality in organotypic culture is a necessity.

In this study, we investigated the viability and functionality of retinal explants in culture conditions. We used an organotypic retinal explant culture system, which was optimized to correspond to the natural environment in the eye and to enable good preservation of retinal structure over time. We followed the viability of retinal explants during the 14-day culture period and focused especially on the preservation of the functionality of retinal neurons by recording their electrical activity. Retinal tissue has been shown to retain its viability in culture environment for a varying number of days.[3,8–10,12,38] Most of this evidence, however, comes from morphologic studies and

thus does not contain information about the preservation of neuronal functionality. The few studies that have involved the electrophysiological assessment of retinal explant cultures have been primarily conducted using single-cell patch-clamp technique.[9,10,38] In our study, the multielectrode array (MEA) technique was used because it allowed us to investigate electrical activities of large neuronal populations simultaneously and provided information on both photoreceptors and retinal ganglion cells (RGCs). Simultaneous recording from tens of electrodes also reduces the time required for one experiment, enables the recordings from several retinal explants at specific time points, and makes possible the detection of changes in the number of RGCs that remain functional in the degenerating retina. In addition, the large number of electrodes allow the recording of an electroretinogram (ERG) in a multifocal manner, revealing information on the local activities of photoreceptors that is challenging to obtain from rodents in vivo.[39–41] Furthermore, the MEA technique typically has an excellent recording stability, and compared to single-cell techniques, this allows the monitoring of the activity of neurons for longer periods. To assess changes in retinal morphology, including neuronal loss and the level of reactive gliosis during the culture, we used immunohistochemical methods. The combination of morphologic and functional characterization gives detailed insight into the changes occurring in retinal organotypic explants during a period of 2 weeks and improves the usability of retinal explant cultures in the future.

Materials and Methods

Animals and Tissue Preparation

Six- to eight-week-old C57Bl/6J mice (Animal Centre, University of Eastern Finland, Kuopio, Finland; and Animal Facility, Tampere University, Tampere, Finland) were used in this study. The animals were housed at a constant temperature (22 ± 1°C) and in a light-controlled environment (lights on from 7 AM to 7 PM). All animals were treated in accordance with the ARVO Statement for the Use of Animals in Ophthalmic and Vision Research and the EC Directive 86/609/EEC for animal experiments, using protocols approved and monitored by the Animal Experiment Board of Finland.

The mice were dark-adapted overnight and killed by CO_2 inhalation and cervical dislocation. Both eyes were immediately enucleated and immersed in oxygenated (95% O_2 and 5% CO_2) Ames' medium. The eyes were opened around the limbus, followed by the removal of the cornea, lens, and the vitreous body. With very fine forceps, the remainders of the vitreous body were gently peeled off, and the neural retina was carefully isolated from the underlying retinal pigment epithelium (RPE). Each retina was cut into two halves, yielding four retinal explants per animal.

Retinal Explant Culture

The retinae were cultured for 14 days in vitro (DIV) using a method developed and optimized by Johnson and Martin[8] and Bull et al.[3] Briefly, the retinal explants were transferred onto 12-mm-diameter culture inserts (0.4 μm pore; EMD Millipore Corp., Billerica, MA, USA) and positioned so that the photoreceptors were facing the insert membrane. The explants were flattened by gently removing the excess medium and cultured at the air-medium interface in serum-free conditions with the following supplements: 2% B27 (0080085-SA; Invitrogen, Carlsbad, CA, USA) and 1% N2 (17502-048; Invitrogen), 2 mM GlutaMAX (35050038; Invitrogen), and 100 units/mL penicillin–100 μg/mL streptomycin (P4333; Sigma-Aldrich Corp., St. Louis, MO, USA), added to medium (Neurobasal-A, 10888022; Invitrogen). Half of the media were changed every 2 days, and the first change occurred at 1 DIV. The cultures were maintained in humidified cell culture incubators at 37°C and in 5% CO_2.

Electrophysiological Recordings

Electrophysiological characterization of the retinae was performed using a MEA technique to record RGC action potentials and transretinal microelectroretinograms (miERGs).[42] The recordings were carried out at specific DIV (0, 1, 2, 4, 7, 10, and 14 DIV), and each explant was recorded at only a single time point. To perform the MEA recordings, the insert membrane with the retinal explant was removed from the insert plate and transferred onto a perforated 60-channel MEA plate (60pMEA200/30iR-Ti; Multi Channel Systems MCS GmbH, Reutlingen, Germany) with the RGCs facing the electrodes. The explant was sandwiched between the culture insert (or small piece of lens paper at 0 DIV) and MEA plate and weighted down by a slice anchor (SHD-41/10; Warner Instruments, Hamden, CT, USA). The diameter of the electrode array was 1.64 mm, and the electrodes were 30 μm in diameter and spaced 200 μm apart. An external reference electrode was placed into the perfusion medium at the photoreceptor side of the retina to enable miERG recordings. The retinae were perfused with oxygenated Ames' solution buffered with sodium bicarbonate and equilibrated with a gas mixture of 95% O_2 and 5% CO_2. The temperature was held at 36°C. All the recordings were conducted inside a light-tight Faraday cage in a room illuminated with dim red light, and all the preceding procedures (tissue preparation and culture) were conducted under dim red light.

For every retina, we used a measurement protocol that enabled the recordings of both spontaneous and light-evoked activity. We started with the recordings of spontaneous activity and proceeded with light-evoked activity with increasing stimulus intensity. As light stimuli, we used pulses of full-field 505-nm light with varying durations and intensities. Our stimulus protocol started with flashes of light (20 milliseconds) and included steps of light with varying durations (1, 3, 5, 10, and 30 seconds). We varied the time interval between light stimuli for each recording. The number of consecutive stimuli in a recording sequence decreased (from 10 to 1), and the interval between each stimulus increased (from 10 to 60 seconds), as the stimulus protocol proceeded. The 30-second stimuli were presented only once at the end of the experiment.

MEA Data Analysis

Signals were acquired using software (MC_Rack; Multi Channel Systems MCS GmbH) at a sampling rate of 20 kHz and were stored for offline analysis. The data were further analyzed with additional software (MC_Rack, NeuroExplorer; Plexon, Inc., Dallas, TX, USA, and MATLAB; MathWorks, Inc., Natick, MA, USA). The recordings were band-pass filtered between 100 and 3000 Hz for the RGC spike responses and low-pass filtered (with a cutoff frequency of 40 Hz) for the miERG response. Spikes were detected using a negative threshold trigger set to five times the standard deviation of the filtered data.

Each MEA electrode typically measures the activity of more than one cell. To separate the different waveforms, the data were spike-sorted using a publicly available spike sorting algorithm, Wave_clus, in MATLAB.[43] One spike waveform from a cluster was assumed to belong to one cell. These clustered spike waveforms were stored as time-stamped spike trains. To monitor the quality of spike sorting, each spike train was

Investigative Ophthalmology & Visual Science

ensured to have clean refractory periods (no interspike intervals below 3 milliseconds). Triphasic spike forms were assumed to be axonal and rejected.[44] The firing rates of spike-sorted cells were calculated by counting the number of spikes in a 60-second recording period, and the data from separate retinae were pooled. Statistical analysis of the differences in the distributions was performed with the Kolmogorov-Smirnov test. The data was stated as mean ± SD.

Tissue Preparation for Morphologic Analysis

For morphologic characterization of retinal explants, the following time points ($n = 9$ at each time point) were used: 0, 2, 3, 7, and 14 DIV. Immediately after tissue preparation (at 0 DIV) or at each of the culture time points, the retina was put into fixative and was fixed with 4% paraformaldehyde in 0.1 M PBS, pH 7.4, overnight. For cryosection analysis, the tissue was embedded into optimal cutting temperature compound (Sakura Finetek Europe BV, Alphen aan den Rijn, The Netherlands), cryosectioned at a thickness of 8 µm using a cryostat (Leica CM 1860; Leica Microsystems Nussloch GmbH, Nussloch, Germany), and mounted on slides (SuperFrost Plus; Gerhard Menzel B.V. & Co. KG, Braunschweig, Germany). For whole-mount analysis, the fixed retinae were rinsed with 0.1 M PBS and processed for immunohistochemistry.

Morphologic Analysis

We analyzed qualitatively and quantitatively the survival of RGCs during the culture from retinal cryosections and whole-mount preparations, focusing on the retinal ganglion cell layer (RGCL). Apoptotic cells were detected by TUNEL staining to detect DNA fragmentation in the retinal sections using an in situ cell death detection kit, according to the manufacturer's instructions (Fluorescein, 11684795910; Sigma-Aldrich Corp.). Cell nuclei were counterstained using 0.1 µg/mL nuclear marker 4′,6-diamidino-2-phenylindole (DAPI) (82320-1; Sigma-Aldrich Corp.).

The amount of ganglion cells and melanopsin-expressing intrinsically photosensitive RGCs (ipRGCs) were detected by staining of RNA-binding protein with multiple splicing (RBPMS) (1:200 1830-RBPMS; PhosphoSolutions, Aurora, CO, USA) and melanopsin (1:2500 AB-M38; Advanced Targeting Systems, San Diego, CA, USA), respectively. The level of gliosis in retinal explants was detected by staining of glial fibrillary acidic protein (GFAP) (1:1000 G3893; Sigma-Aldrich Corp.). Secondary antibodies were used (1:500, Alexa Fluor 488 and 594 IgG; Thermo Fisher Scientific, Waltham, MA, USA). All immunostained samples were qualitatively analyzed and imaged using a microscope (AxioImager 2; Carl Zeiss Microscopy GmbH, Jena, Germany). The number of RGCs and apoptotic cells in RGCL were quantified by counting the RBPMS- and TUNEL-positive cells from 6 to 13 widefield fluorescence images of retinal cryosections, and the RGC density was determined by counting RBPMS-positive cells from 8 to 10 confocal images of retinal whole mounts. The images were acquired from three explants at each time point, and quantification was conducted by using ImageJ software (http://imagej.nih.gov/ij/; provided in the public domain by the National Institutes of Health, Bethesda, MD, USA). Statistical analysis of the differences in the cell numbers was performed with the Kruskal-Wallis test. The data were stated as mean ± SD.

Microscopy was performed with a laser-scanning confocal microscope (Zeiss LSM780; Carl Zeiss Microscopy GmbH) mounted on inverted microscope body (Zeiss Cell Observer; Carl Zeiss Microscopy GmbH) by using Plan-Apochromat 63×/1.4 oil immersion or Plan-Apochromat 25×/0.8 multi-immersion objectives (Carl Zeiss Microscopy GmbH). Voxel size was set to $x = y = 100$ nm, $z = 200$ nm and image size to 1024 × 1024 pixels (63× objective) or $x = y = 550$ nm, $z = 500$ nm and image sizes to 1024 × 1024 or 2048 × 2048 pixels (25× objective).

Widefield microscopy was performed with fluorescence microscope (Nikon Eclipse FN1; Nikon, Amsterdam, Netherlands) by using CFI Super Fluor 40×/1.3 oil immersion objective (Nikon) and pixel size $x = y = 325$ nm and image size of 1024 × 1024 pixels. The images were saved in czi-format (confocal micrographs) or nd2-format (widefield micrographs) and processed with ImageJ software, adjusting linearly only brightness and contrast.

Results

Electrical Activity of Freshly Isolated Retinae

Two types of electrical activities were recorded from freshly isolated retinae using the MEA technique (Fig. 1). When the retinal explant was exposed to a light stimulus, the unfiltered signal included both ganglion cell spike responses and transretinal miERG (Fig. 1A). These responses can be separated from each other by filtering the signal: low-pass filtering isolates the miERG (Fig. 1B) and band-pass filtering isolates the RGC spike responses (Fig. 1C). Typical of transretinal ERG in general, the waveform of the miERG was multiphasic with negative a-wave and positive b-wave components arising primarily from the functioning of photoreceptors and bipolar cells, respectively.[45,46] A slow negative wave component is also typically present in transretinal ERG, resulting from the activity of Müller glial cells.[45,47] However, this was only a minor wave component in our recordings. The amplitude and kinetics of the a-wave showed stimulus light-dependent behavior so that with increasing light intensity the time to peak decreased and the amplitude increased until reaching a saturation level.

Electrophysiological recordings of RGC activity are often plotted using raster plots, where the ticks represent the detected spikes in the recordings. In darkness, RGCs exhibit spontaneous firing, which in the freshly isolated retinae was rich and diverse (Fig. 1D). Examples of raster plots of light-evoked activity with varying stimulation lengths from individual RGCs are shown in Figure 1E. In the examples, on-type ganglion cells respond to light increments with increased spiking and off-type ganglion cells with decreased spiking, typical of their natural behavior. Overall, the mouse retina has been shown to contain more than 30 distinct RGC types based on their morphology and/or responses to light,[48,49] and in our recordings this was reflected by the diversity of RGC spike train characteristics.

Spontaneous Activity of RGCs During the Culture

Retinal functionality was followed during a 14-day culture period at 1, 2, 4, 7, 10, and 14 DIV time points. The MEA technique enabled the analysis of the overall condition of the RGCs in the retina due to its capability to record from multiple electrodes simultaneously. Spontaneous RGC activity was present during the whole culture period, although it gradually changed and diminished. This is illustrated in Figure 2 as representative spike trains (Fig. 2A), cumulative firing rate histograms (Fig. 2B), and spike activity parameters (Figs. 2C–2G).

The percentage of active MEA channels decreased from 73.1% ± 9.5% to 9.4% ± 8.8% during the culture (Fig. 2D). Spike trains from one to three cells, separated by spike sorting, were recorded simultaneously from each electrode. The

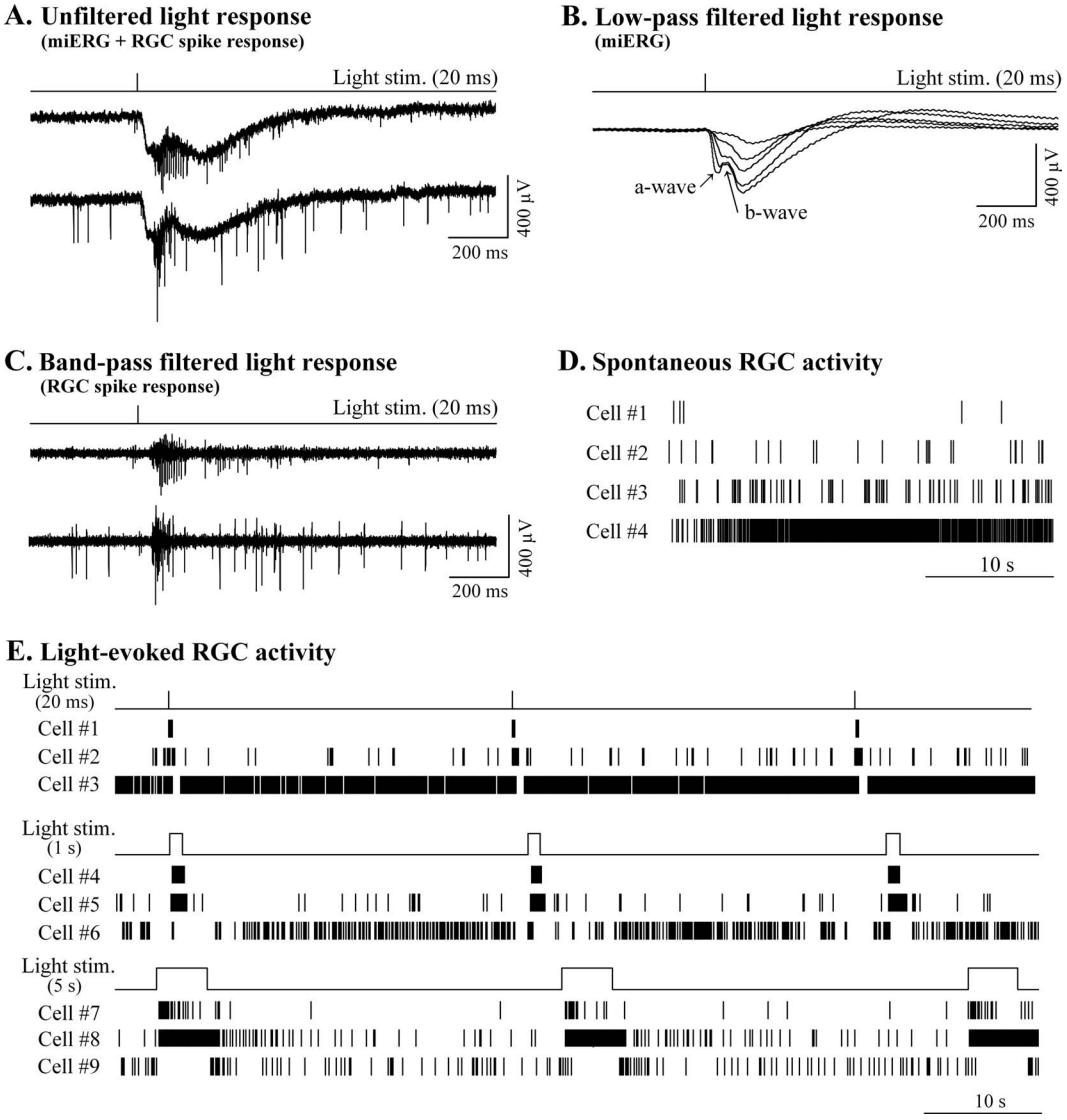

Figure 1. Electrical activity of freshly isolated retinae (0 DIV). (**A**) Examples of unfiltered signals recorded simultaneously from two separate channels when a retinal explant was exposed to a 20-millisecond full-field light stimulus (505 nm, 2.1×10^6 photons μm^{-2}). The signals include both ganglion cell spike responses and transretinal miERG. (**B**) An example of the miERG response family recorded from a single channel as a response to 20-millisecond full-field light stimuli at increasing intensities (from 2.1×10^5 photons μm^{-2} (topmost trace) to 2.1×10^7 photons μm^{-2} (lowest trace). Signals are low-pass filtered with the cutoff frequency of 40 Hz. (**C**) RGC spike activity from two different channels separated from the unfiltered signals (presented in **A**) by band-pass filtering between 100 and 3000 Hz. (**D**) Representative raster plots of spontaneous RGC activity from four different cells recorded simultaneously for 30 seconds. The examples are chosen to represent mean firing rates of quarters (25%, 50%, 75%, and maximum) of the cumulative firing rate histogram of the spontaneous RGC activity. (**E**) Raster plots of light-evoked RGC activity from nine different cells. Full-field light stimulus (2.6×10^9 photons μm^{-2} s^{-1}) with varying pulse lengths (20 millisecond, 1 second, and 5 second) is used as a light stimulus.

number of simultaneously recorded cells per retinal explant was initially 53.0 ± 4.0. This number decreased during the 14-day culture period to 2.5 ± 7.0 (Fig. 2E). Based on the recorded waveforms, triphasic spikes were regarded as axonal spikes. During the first week in culture, the number of cells per retinal explant with axonal responses decreased from 6.5 ± 0.9 to 0.5 ± 0.4, and after the 7 DIV time point, triphasic spike waveforms were not detected (Fig. 2E). RGC response peak-to-peak amplitudes decreased during the 2-week culture period so that the mean value changed from 82.4 ± 0.8 to 67.9 ± 1.8 µV and the maximum value from 229 ± 47 to 76 ± 62 µV (Fig. 2F). The peak-to-peak amplitudes, however, showed a temporal increase from 1 DIV to 2 DIV: maximum and average amplitudes increased from 218 ± 46 to 279 ± 66 µV and 84.8 ± 0.8 to 102.7 ± 1.0 µV, respectively.

The firing rate distributions of spontaneous RGC activity changed during the culture (Fig. 2B), and the change compared to 0 DIV was statistically significant after 4 DIV ($P < 0.05$). Overall, the change in the firing rate distributions was seen as an increase in low-frequency values (firing rates ≤2 Hz) and as a decrease in high-frequency values (firing rates >2 Hz) during the culture, with the 2 DIV time point deviating from this behavior (Fig. 2G). The mean firing rates of spontaneous activity decreased from 2.7 ± 0.6 to 0.5 ± 0.4 Hz during the follow-up (Fig. 2C). However, the mean firing rate increased from 1 DIV to 2 DIV (from 1.4 ± 0.4 to 3.2 ± 0.6 Hz), reaching a value that was even higher than that recorded from the

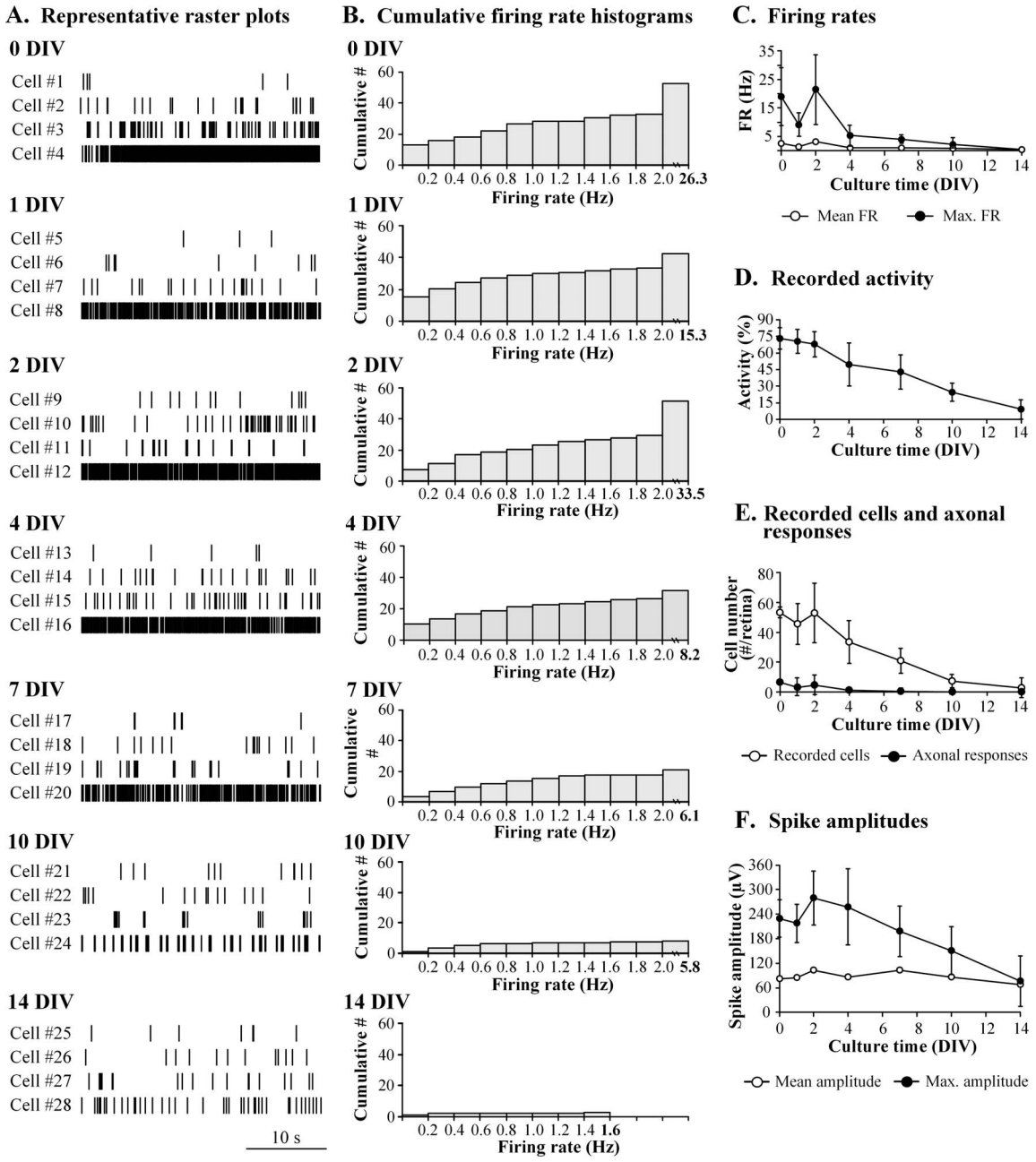

Figure 2. Spontaneous RGC activity during the 14-day culture period. (**A**) Representative raster plots of spontaneous RGC activity from four different cells recorded simultaneously for 30 seconds at 0, 1, 2, 4, 7, 10, and 14 DIV. The examples are chosen to represent mean firing rates of quarters of the cumulative firing rate histograms (25%, 50%, 75%, and maximum). (**B**) Distributions of mean firing rates of spontaneous RGC activity at 0, 1, 2, 4, 7, 10, and 14 DIV. The distributions comprise the cumulative number of mean firing rates of all cells on each recording day. The mean firing rates were calculated by counting the number of spikes in 1-second time windows over a 60-second recording period, and the data from separate retinae are pooled. The histograms show the cumulative number of mean firing rates at different frequencies in 0.2-Hz bins from 0 Hz to the maximum value of mean firing rate for each recording day. The last *bar* represents all mean firing rates between 2 Hz and the maximum mean firing rate (*bolded*) on that recording day. (**C**) Averages of mean and maximum firing rates of spontaneous RGC activity on each recording day. (**D**) Recorded activity during the culture as a percentage of active channels. (**E**) Number of recorded cells (number/retina) and axonal responses (number/retina) during the culture. (**F**) Average and maximum spike amplitudes during the culture (peak-to-peak, microvolts). (**G**) Proportion of RGCs (percentage) with mean firing rates at low (≤2 Hz) and high (>2 Hz) frequencies during the culture. The whiskers show standard deviation of the means for each recording day ($n = 3$–4).

freshly isolated retinae. The maximum firing rates of spontaneous activity decreased during the culture on average from 19.1 ± 10.1 to 0.5 ± 0.7 Hz, with the exception of an increase between 1 DIV and 2 DIV of 9.1 ± 4.2 to 21.6 ± 12.0 Hz.

Light-Evoked Activity of Retinal Cells During the Culture

Light responsiveness of retinal explants was assessed by measuring the light-evoked activity of the retinal cells during the culture. The responsiveness of photoreceptors to light stimulation (miERG response) was detectable for the first 2 days following retina isolation (Figs. 1B, 3A). In the RGC level, however, light responsiveness was retained for much longer, even for 7 days (Figs. 3B, 3C). Figure 3 presents examples of light-evoked retinal activity as responses to rod-saturating light stimuli (intensity of 2.6×10^9 photons μm^{-2} s^{-1}) ranging from 20-millisecond flashes to 1- or 10-second steps of light. Between 0 DIV and 2 DIV, we could detect light responses with all stimulus lengths; however, the 20-millisecond stimulus did not induce a visible response after 2 DIV. Furthermore, with increasing culture time, longer steps of light were needed to induce a response in RGCs. After 7 days in culture, no direct response to light stimulation was observed, even with the highest intensity and the longest stimulus duration.

Distributions of Population Firing Rates of Light-Evoked RGC Activity During the Culture

The effect of light stimuli on RGC activity was seen as an increase in the amount of recorded cells during the measurement protocol in the whole culture period (Fig. 4C). At the 0 DIV time point, the number of recorded cells per retinal explant increased from spontaneously active 53 ± 4 cells to 69 ± 1 and 66 ± 2 active cells during stimulation by flashes and steps of light, respectively. At the end of the 14-day culture period, electrical activity of 4 ± 3 and 11 ± 9 cells were recorded in the presence of light stimulation (flashes and steps, respectively) compared to spontaneously active 2 ± 2 cells. In addition to increased RGC activity, light stimulation changed distributions of population firing rates (Figs. 4A, 4B). This was seen as a decrease in low-frequency values (≤2 Hz), as an increase in high-frequency values (>2 Hz), and as an increase in the average values of mean and maximum firing rates (Figs. 4D, 4E). Most of these effects were more evident during the first 4 days in culture. From 7 DIV on, light-induced changes in the mean firing rates were less clear. However, the light stimulation induced an increase in the maximum firing rate during the whole culture period, with the exception at 2 DIV (Fig. 4E).

Changes in Morphology During the Culture

To follow the morphology changes in the retinal explants during the culture, we performed assays to detect the amount of apoptotic cells in the retinal explants and the number of RGCs in the RGCL. A TUNEL assay was used to identify and quantify apoptotic cells in retinal cryosections (Fig. 5A). The assay indicated a high number of TUNEL-positive cells present in different retinal layers already at 3 DIV. At this time point, the majority of TUNEL-positive cells were localized in the inner nuclear layer (INL). In addition, some cells in the outer nuclear layer (ONL) and RGCL were also TUNEL positive. At 7 DIV, we observed the overall highest density of TUNEL-positive cells in retinal sections from which the TUNEL positivity decreased toward the 14 DIV time point. We quantified the number of TUNEL-positive cells in the RGCL, and based on 6 to 13 widefield fluorescence images at each time point, it increased during the 14-day culture from 0 to 33 ± 6 cells/300 μm (Fig. 5B). The highest density of TUNEL-positive cells was observed at 7 DIV (38 ± 5 cells/300 μm). The increase in TUNEL-positive cells was coupled with a decrease in the number of RGCs during the culture. Based on the number of RBPMS-positive cells in the retinal cryosections (6 to 13 widefield fluorescence images at each time point), the number of RGCs decreased during the first 2 days from 49 ± 9 cells/300 μm to 31 ± 9 cells/300 μm (statistically significant difference, $P < 0.01$). By the end of the 14-day culture, the number of RGCs had decreased to 24 ± 5 cells/300 μm (statistically significant difference compared to 0 DIV, $P < 0.01$). It is noteworthy that the amount of apoptotic cells exceeded the number of RGCs at the 7 and 14 DIV time points.

More precise evaluation of the change in RGC density was performed from the whole-mount preparations (Fig. 5C). Quantification of RGCs (RBPMS-positive cells) from 8 to 10 confocal images at each time point revealed that the RGC density decreased during the first 2 days in culture by 21% (1400 ± 600 cells/mm^2 at 0 DIV versus 1100 ± 400 cells/mm^2 at 2 DIV). After the first week in culture, the RGC density had declined by 50% (to 700 ± 200 cells/mm^2), and during the whole 14-day period, the amount of RGCs had decreased by 70% (to 400 ± 200 cells/mm^2), both changes with a statistically significant difference, $P < 0.01$. From the RGC population, the existence of melanopsin-expressing ipRGCs during the culture was assessed by staining melanopsin from the retinal whole mounts and cryosections (Fig. 6) and analyzing both immunoreactivity and cell morphology.[50] The ipRGCs were present in the explants at all the time points from 0 to 14 DIV, with examples at 0, 2, 7, and 14 DIV shown in Figure 6A. Since ipRGCs present a small proportion of neurons among the total RGC population, we were unable to reliably quantify changes in their number during the culture.

As a part of our morphologic analysis, we analyzed the level of gliosis in retinal explants during the culture. In general, gliosis is characterized as the proliferation and hypertrophy of glial cells, and it is one of the earliest and most remarkable responses of the retina to various stress factors.[51–54] In the mammalian retinae, gliosis results in upregulation of the expression of intermediate filament proteins, such as GFAP.[52,54,55] GFAP immunostaining from whole-mount preparations showed typical retinal astrocyte labeling at both 0 and 3 DIV (Fig. 6B). Severe retinal gliosis was observed at 7 DIV and persisted for the remaining culture period up to 14 DIV, extending through the retina (Fig. 6C). It is of interest that when strong gliosis was present in the 14 DIV explants, ipRGC immunoreactivity was especially intense, and the ipRGC processes were clearly detectable in the close vicinity of the glial cell processes (Fig. 6C).

Discussion

Organotypic retinal explant cultures provide cost-effective and reproducible in vivo mimicking tools for investigations of retinal functions and for the development of novel retinal therapies.[2,23,25,30,34,56–64] For the full exploitability of the explant cultures, however, viability of retina in culture conditions needs to be thoroughly characterized. While most previous studies have focused on morphology, the maintenance of retinal functionality in culture conditions has remained unclear. To fill this gap in knowledge, we investigated the structural and functional integrity of organotypic retinal explants in culture conditions by evaluating both retinal morphology and functionality during the 2-week culture.

The preparation of retina for organotypic explant culture, which requires axotomy of the optic nerve and separation of

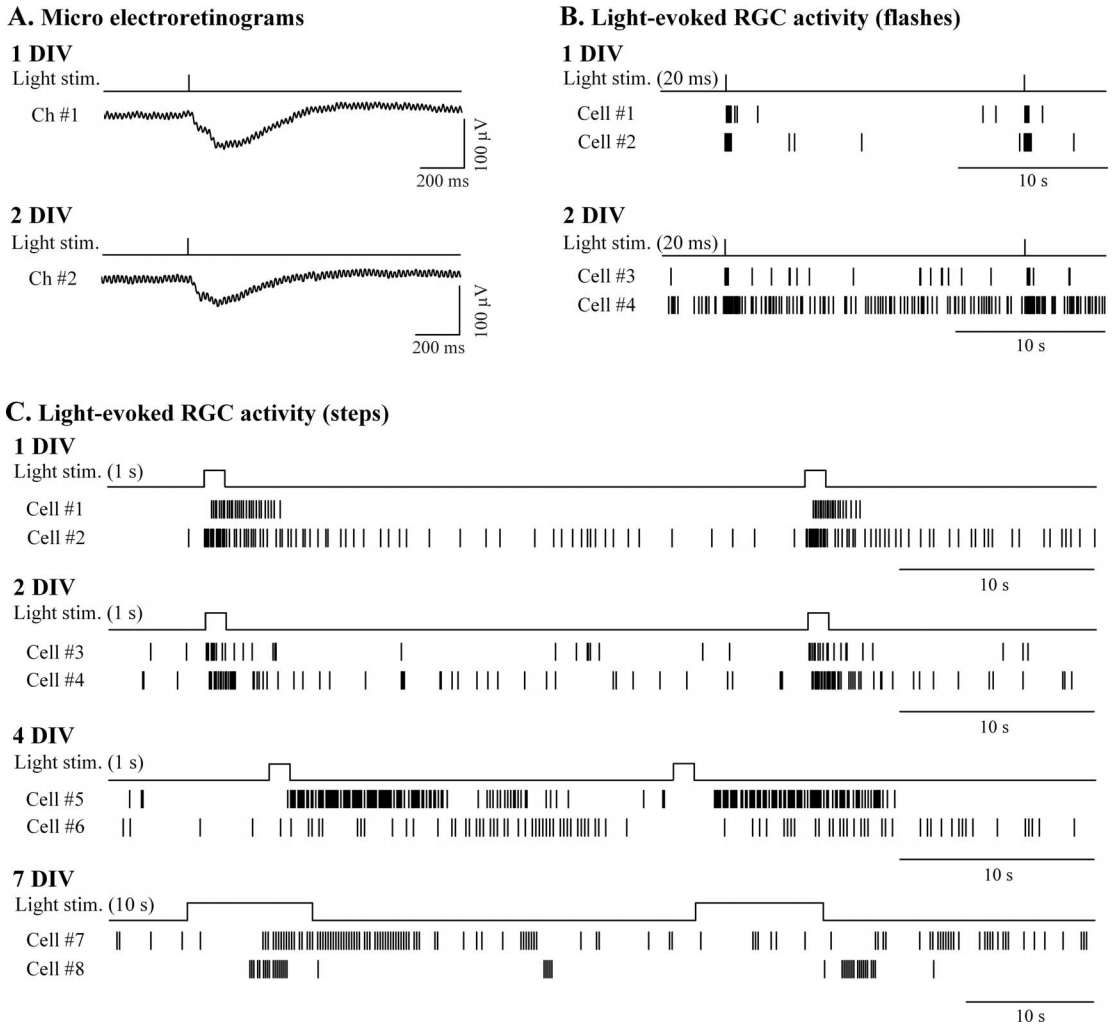

FIGURE 3. Light-evoked activity of different retinal cells during the culture. (**A**) Examples of miERG responses recorded from a single channel as a response to 20-millisecond full-field light stimuli (intensity of 4.2×10^6 photons μm^{-2}). Signals are low-pass filtered with the cutoff frequency of 40 Hz. The miERG responses were not detectable after 2 DIV. (**B**) Examples of RGC light responses to two successive flashes of light (20-millisecond duration, 20-second interval). A flash of light did not induce a visible response after 2 DIV. (**C**) Examples of RGC light responses to two successive steps of light (at 1 to 2 DIV: 1-second duration, 30-second interval; at 4 DIV: 1-second duration, 30-second interval; and at 7 DIV: 10-second duration, 20-second interval). The intensity of light stimulus in flashes and steps was 2.6×10^9 photons $\mu m^{-2} s^{-1}$.

the neural retina from the RPE, results in cellular changes throughout the retina.[65,66] The morphologic changes are highly similar to those following retinal detachment or axotomy in vivo. In vitro, the cultured retinal explants have been reported to become thinner and suffer from a loss of major retinal neuron types after 4 to 7 DIV.[3,12,66,67] Similar to these results, we observed clear temporal changes in the retinal explants during the culture in both morphology and functionality. We detected apoptotic cells in the cultures at 3 DIV, with their prevalence peaking at 7 DIV. These changes were accompanied by loss of RGCs during the culture. The functional changes were analyzed both in the retinal input and output levels, thus including the activity of retinal photoreceptors and RGCs. The presence of spontaneous RGC activity for the whole 14 DIV culture period and light-evoked RGC activity up to 7 DIV is very promising for the usability of explant cultures in long-term studies, for example, in the development of novel therapies for diseases of optic nerve, such as glaucoma.

The first degenerative changes in the retinal explant cultures have been reported to occur in photoreceptors, starting from the gradual loss of their outer and inner segments followed by the loss of photoreceptor nuclei.[12,65] In this study, the preservation of photoreceptor functionality was followed by transretinal miERG, and a photoreceptor response was detectable up to 2 DIV. It is worth noting that the transretinal ERG response is induced by photoreceptors but reflects the light-induced changes in the radial currents of the retina, representing all retinal cells and circuits.[44] Furthermore, the method enables measuring the mass response of retinal cells but is not sensitive when evaluating the responses at the level of individual neurons or detecting RGC activity induced by photoreceptor input. Thus, in the degenerating retina, photoreceptor viability cannot be fully assessed using ERG exclusively due to the changes occurring throughout the retina. In the present work, although we were not able to detect miERG response after 2 DIV, our MEA recordings indicated retinal light responsiveness for longer than 2 DIV. Moreover, TUNEL assay illustrated that apoptotic cells were present in the photoreceptor nuclei layer starting from 3 DIV, with the highest amount of apoptotic cells in the ONL observed at 7 DIV. The same time range of photoreceptor survival has been reported in previous studies, with the observation of photoreceptor outer segment deterioration

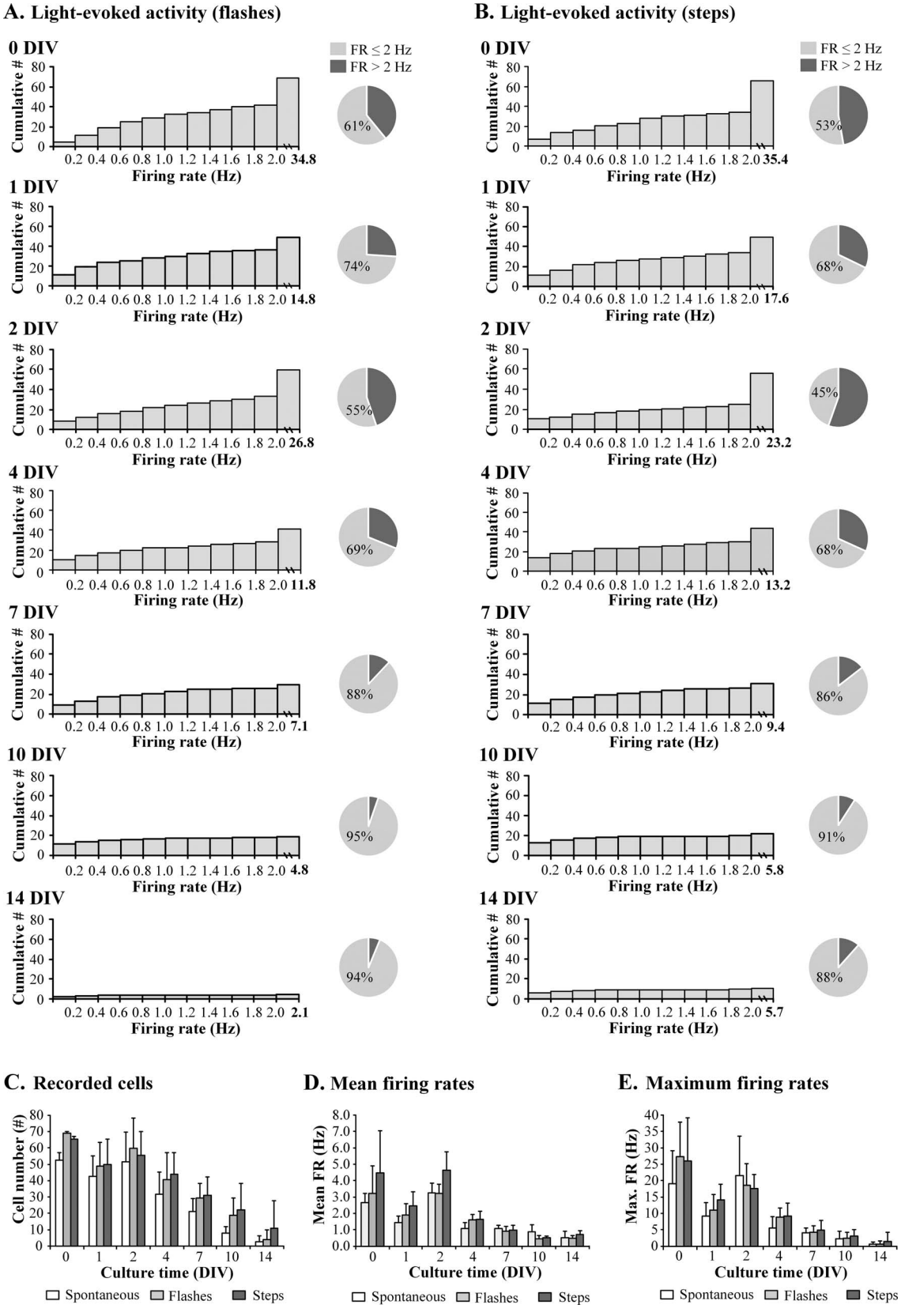

FIGURE 4. Distributions of mean firing rates of light-evoked RGC activity at 0, 1, 2, 4, 7, 10, and 14 DIV. The cumulative distributions comprise the mean firing rates of all cells on each recording day over a 60-second recording period, and the data from separate retinae are pooled. (**A**, **B**) Cumulative histograms of light-evoked activity as response to flashes and steps of light during the culture. The histograms show the number of mean firing rates at different frequencies in 0.2-Hz bins from 0 Hz to the maximum value of mean firing rate for each culture day. The last bar represents mean firing rates between 2 Hz and the maximum mean firing rate (*bolded*) on that culture day. The pie charts show proportions of

RGCs (percentage) with mean firing rates at low (≤2 Hz) and high (>2 Hz) frequencies during the culture. (**C**) Number of recorded cells (number/retina) in spontaneous and light-evoked RGC activity during the culture. (**D**, **E**) Averages of mean and maximum firing rates of spontaneous and light-evoked RGC activity during the culture. The whiskers show standard deviations of the means for each recording day ($n = 3$–4). The intensity of the light stimulus was 2.7×10^9 photons μm^{-2} s^{-1}, and the duration of a single light stimulus was 20 millisecond in flashes and 1 second in steps.

after 3 DIV and the most significant loss of photoreceptors between 3 and 8 DIV.[5,67] The main reason for the poor survival rate of photoreceptors is the absence of RPE, which performs many vital support and maintenance functions for the retina and photoreceptors.[68] To overcome this challenge, retina-RPE cocultures have been suggested as ways to improve photoreceptor cell survival[69–73] (Szabo A, *IOVS* 2018;59:ARVO E-Abstract, 4021).

In the ganglion cell layer, the death of RGCs following axotomy has been reported both in vitro and in vivo in rodents, rabbits, and humans.[3,59,74–76] Our analysis of the RGC density revealed that the number of RGCs in the retinal explants gradually decreased during the 14-day culture period. At 2 DIV, the number of RGCs had decreased by 21%. After the first week in culture, the RGC number had halved, with a further decrease resulting in 70% RGC loss by 14 DIV. Our results are consistent with the earlier studies that demonstrate the loss of RGCs in retinal explants to be most rapid during the first week in culture, after which the rate of loss becomes slower.[3,59,76] On the other hand, morphologic studies of RGCs in vivo have shown these cells to survive for 5 to 7 days after axotomy, followed by a significant loss in RGC survival during the subsequent days.[74,75]

Functional studies of rat RGCs have indicated their firing rates to decrease 7 days after axotomy.[24] Patch clamp recordings from retinal explant cultures have revealed that rat and rabbit RGCs are able to generate action potentials up to 4 to 6 DIV and exhibit light response up to 4 DIV.[9,10] In

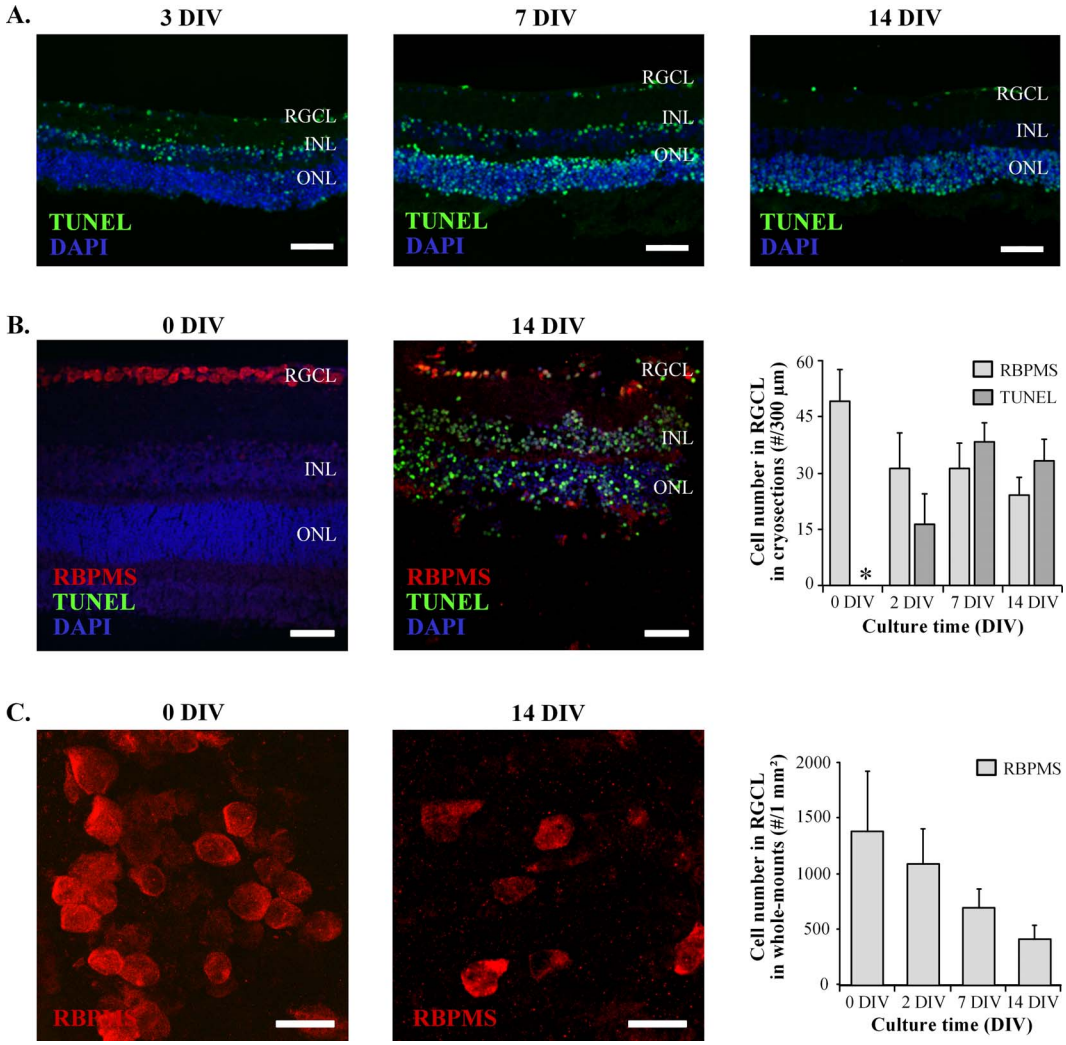

Figure 5. Changes in the morphology of the retinal explants during culture. (**A**) Retinal cell nuclei and apoptotic cells in cryosections at 3, 7, and 14 DIV time points. TUNEL-positive cells are shown in *green* and cell nuclei (DAPI) in *blue*. INL, inner nuclear layer; ONL, outer nuclear layer. (**B**) Confocal images of RBPMS (*red*) and TUNEL-positive cells (*green*) in retinal cryosections at 0 and 14 DIV time points. The number of RGCs and apoptotic cells in RGCL was quantified by counting the RBPMS and TUNEL-positive cells from widefield fluorescence images (mean ± SD, $n = 6$–13).* No TUNEL positivity at the 0 DIV time point. (**C**) RBPMS-positive cells (*red*) in retinal whole mounts at 0 and 14 DIV time points. The number of RGCs was quantified by manually counting the RBPMS-positive cells from the confocal images (mean ± SD, $n = 8$–10). *Scale bars*: 50 µm (**A**, **B**) and 20 µm (**C**).

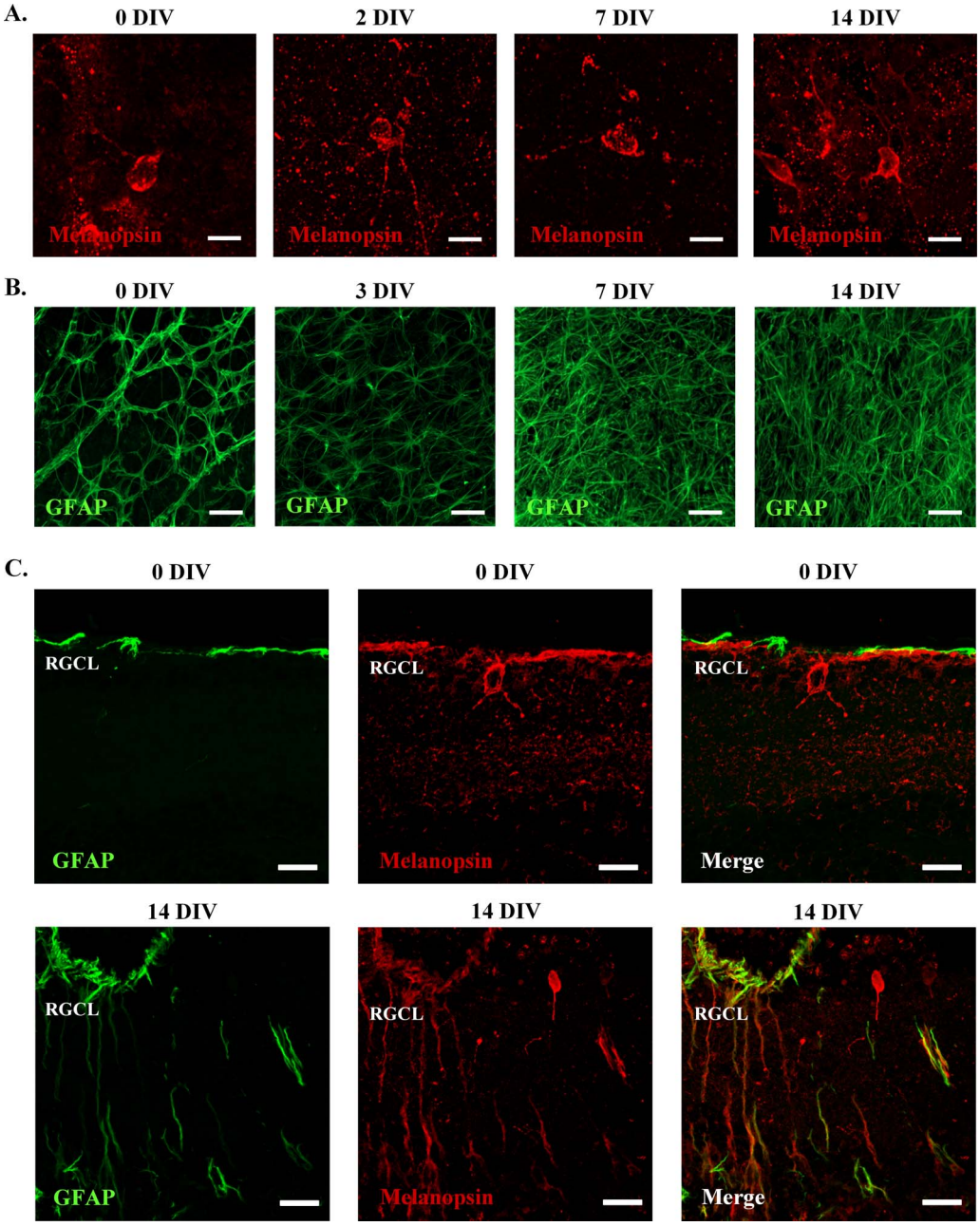

FIGURE 6. The presence of ipRGCs (**A**, **C**) and reactive gliosis (**B**, **C**) in the retinal explants during culture. (**A**) Maximum intensity projections of confocal images showing melanopsin immunostaining (*red*) in retinal whole mounts. Melanopsin-positive cells with characteristic ipRGC morphology indicate the presence of ipRGCs in retinal explants at 0, 2, 7, and 14 DIV time points. (**B**) Immunostaining of GFAP (*green*), labeling the intermediate filaments in glial cells in retinal whole mounts at 0 DIV, 3 DIV, 7 DIV, and 14 DIV time points. (**C**) GFAP (*green*) and melanopsin (*red*) immunostaining in retinal cryosections at 0 and 14 DIV time points. Maximum intensity projections of confocal images show the presence of ipRGCs in the RGCL and GFAP-positive glial cell processes at the inner surface of the retina at 0 DIV. At 14 DIV, ipRGCs and their processes are detected especially strongly in the areas with severe gliosis. *Scale bars*: 10 μm (**A**), 50 μm (**B**), and 20 μ (**C**).

addition, patch clamp recordings of zebrafish retinal cultures have demonstrated RGCs to be viable up to 10 DIV and to evoke light responses until at least 2 DIV.[38] In the present work, we observed the presence of gradually diminishing RGC activity with temporally changing distribution of RGC firing rates up to 14 DIV. The MEA technique used enabled us to follow the functionality of the RGC populations, although we cannot fully exclude the contribution of displaced amacrine cells in the recordings.[77,78] However, due to the small size of amacrine cell spike amplitudes (rarely bigger than 25 mV) and frequency content below 80 Hz, our recordings with a band-pass filter of 100 to 3000 Hz should remove such spikes from our data.[79]

MEA technique has been used with retinal explant cultures previously to provide a brief overview of rabbit RGC responses to spatial white noise stimuli after 2 to 3 days in culture.[9] At this time point, RGCs in explant cultures showed slightly reduced light responsiveness that was visible as decreased mean firing rates and an increased number of cells with mean firing rates at low frequencies (<2 Hz). Similarly, in our study, light-evoked RGC responses started to reduce at the 1 DIV time point, so that the mean firing rates decreased and the number

of cells with mean firing rates at low frequencies (<2 Hz) increased during the whole culture period. An exception to this was the time point at 2 DIV when light-evoked RGC activity was at the same level as it was initially. However, this time point also differed in spontaneous RGC activity as we observed it to increase in the 2 DIV explants. This was seen as an increased number of recorded cells, larger spike amplitudes, and increased high-frequency firing compared to 1 DIV explants. Increased spontaneous RGC activity has been reported during photoreceptor degeneration in different animal strains, including rd1 and rd10 mice.[57,80–83] It has been suggested that rhythmic and increased RGC activity in the mature retina is triggered by missing photoreceptor input.

When the functional data and morphologic RGC survival were compared, the observed changes were surprisingly similar during the first week in culture. The number of RGCs with spontaneous and/or light-evoked electrical activity decreased concurrently with the RGC density. After 2 DIV, the number of electrically active cells had decreased by 15%, and RGC density by 21%. By the end of the first week, both of these numbers had halved (active cells by 53% and RGC density by 50%). After 2 weeks in culture, however, the number of RGCs that showed activity in MEA recordings had dropped more than the RGC density: the decrease in recorded RGCs was 84% whereas the decrease in RGC density was 70%. This indicates better structural preservation of retinal explants in long-term culture and suggests that the cells most likely lose their functionality before they actually die.

In our MEA recordings, light-evoked RGC activity was present up to 7 DIV. Even though we were not able to detect miERG response from photoreceptors up to this time point, the preservation of the ONL indicates their survival and suggests their contribution to the RGC light responsiveness. Furthermore, it is noteworthy that the ipRGCs function as a third class of light-sensitive neurons in the retina.[84–87] They constitute 1% to 5% of the total RGC population in mice, and their light responses have specific characteristics such as long latency, long temporal integration, slow deactivation, and sustained response under tonic light stimulation.[50,85,87,88] Some of these response characteristics were evident in our MEA recordings, being even more prominent during the 4 to 7 DIV culture period. This suggests that the light-driven RGC activity observed during the later culture time points most likely reflects the activity of the ipRGCs. It is interesting that several studies have shown ipRGCs to be more resistant to cell death and injury than conventional RGCs,[89] and our results do not contradict with these observations. By immunostainings, we could detect ipRGCs in our retinal explants up to 14 DIV; however, due to their relatively small number, we were unable to reliably quantify changes in their expression during culture.

The upregulation of GFAP is universally used as a cellular marker for retinal injury.[55] Studies on organotypic cultures from mouse retinae have shown GFAP to be upregulated from 2 to 3 DIV and to peak at 6 to 8 DIV.[12,38] In our study, severe gliosis was observed at 7 DIV onward, making individual astrocytes difficult to distinguish. Studies show reactive gliosis as a highly variable disease-dependent response that can be either supportive or harmful to the retina, depending on the injury or disease.[60,90–94] It of interest that astrocytes could participate in the clearance of the RGC axonal debris.[95] Moreover, Müller glial cells have been demonstrated as a source of neuronal regeneration after retinal damage in mammals, suggesting their potential in retinal therapies.[96,97] The presence of RGC activity at the later time points with severe gliosis might be partially a result of the supportive effects of glia to the retina. Further indication of this supportive role was the observation of the ipRGC processes, especially in the areas with strong gliosis. However, it is possible that the diminishing RGC activity during the culture is partly the result of increased density of glial cells that can prevent the measurement of electrical signals from RGCs with the MEA system. Yet, mean spike amplitudes of spontaneous RGC activity were quite constant during the culture, suggesting that the increased number of glial cells does not significantly attenuate the signals.

In this study, we have characterized the preservation of retinal viability in culture conditions. Our electrophysiological and immunohistochemical data demonstrates the changes that occur to retinal functionality and morphology when cultured as an organotypic explant. The observation of neuronal electrical activity for the whole 2-week culture period is very promising for the future use of explant cultures in retinal studies and therapy development.

Acknowledgments

The authors thank Gregory Schwartz (Northwestern University), Teemu Ihalainen (Tampere University), and Julia Johansson (Tampere University) for their valuable comments on the manuscript and AnneMari Haapaniemi for technical assistance. We also thank the Tampere Imaging Facility and Tampere Facility of Electrophysiological Measurements for their support.

Supported by the Academy of Finland (Grants 287287 [SN], 294054 [SN], and 298638 [JH], Emil Aaltonen Foundation, iBioMEP Graduate School, and the Doctoral Programme of TUT's President.

Disclosure: **V. Alarautalahti**, None; **S. Ragauskas**, Experimentica Ltd. (E); **J.J. Hakkarainen**, Experimentica Ltd. (E); **H. Uusitalo-Järvinen**, None; **H. Uusitalo**, None; **J. Hyttinen**, None; **G. Kalesnykas**, Experimentica Ltd. (E); **S. Nymark**, None

References

1. Shamir ER, Ewald AJ. Three-dimensional organotypic culture: experimental models of mammalian biology and disease. *Nat Rev Mol Cell Biol*. 2014;15:647–664.
2. Li Y, Zhang Y, Qi S, Su G. Retinal organotypic culture—a candidate for research on retinas. *Tissue Cell*. 2018;51:1–7.
3. Bull ND, Johnson TV, Welsapar G, DeKorver NW, Tomarev SI, Martin KR. Use of an adult rat retinal explant model for screening of potential retinal ganglion cell neuroprotective therapies. *Invest Ophthalmol Vis Sci*. 2011;52:3309–3320.
4. Caffé AR, Ahuja P, Holmqvist B, et al. Mouse retina explants after long-term culture in serum free medium. *J Chem Neuroanat*. 2001;22:263–273.
5. Fernandez-Bueno I, Fernández-Sánchez L, Gayoso M, García-Gutierrez M, Pastor J, Cuenca N. Time course modifications in organotypic culture of human neuroretina. *Exp Eye Res*. 2012;104:26–38.
6. Ferrer-Martín R, Martín-Oliva D, Sierra A, et al. Microglial cells in organotypic cultures of developing and adult mouse retina and their relationship with cell death. *Exp Eye Res*. 2014;121:42–57.
7. Gancharova O, Manskikh V, Zamyatnin A, Philippov P. Organotypic culture of neural retina as a research model of neurodegeneration of ganglion cells. *Biochem (Mosc)*. 2013;78:1280–1286.
8. Johnson T, Martin K. Development and characterization of an adult retinal explant organotypic tissue culture system as an in vitro intraocular stem cell transplantation model. *Invest Ophthalmol Vis Sci*. 2008;49:3503–3512.
9. Koizumi A, Zeck G, Ben Y, Masland R, Jakobs T. Organotypic culture of physiologically functional adult mammalian retinas. *PLoS One*. 2007;2:e221.
10. Moritoh S, Tanaka K, Jouhou H, Ikenaka K, Koizumi A. Organotypic tissue culture of adult rodent retina followed by

particle-mediated acute gene transfer in vitro. *PLoS One*. 2010;5:e12917.

11. Niyadurupola N, Sidaway P, Osborne A, Broadway D, Sanderson J. The development of human organotypic retinal cultures (HORCs) to study retinal neurodegeneration. *Br J Ophthalmol*. 2011;95:720–726.
12. Müller B, Wagner F, Lorenz B, Stieger K. Organotypic cultures of adult mouse retina: morphologic changes and gene expression. *Invest Ophthalmol Vis Sci*. 2017;58:1930–1940.
13. Wang J, Kolomeyer A, Zarbin M, Townes-Anderson E. Organotypic culture of full-thickness adult porcine retina. *J Vis Exp*. 2011;49:2655.
14. Demas J, Eglen SJ, Wong R. Developmental loss of synchronous spontaneous activity in the mouse retina is independent of visual experience. *J Neurosci*. 2003;23:2851–2860.
15. Engelsberg K, Ehinger B, Wasselius J, Johansson K. Apoptotic cell death and microglial cell responses in cultured rat retina. *Graefes Arch Clin Exp Ophthalmol*. 2004;242:229–239.
16. Thangaraj G, Greif A, Layer P. Simple explant culture of the embryonic chicken retina with long-term preservation of photoreceptors. *Exp Eye Res*. 2011;93:556–564.
17. Biswas S, Haselier C, Mataruga A, Thumann G, Walter P, Müller F. Pharmacological analysis of intrinsic neuronal oscillations in rd10 retina. *PLoS One*. 2014;9:e99075.
18. Busskamp V, Duebel J, Balya D, et al. Genetic reactivation of cone photoreceptors restores visual responses in retinitis pigmentosa. *Science*. 2010;329:413–417.
19. Fischer D, Pavlidis M, Thanos S. Cataractogenic lens injury prevents traumatic ganglion cell death and promotes axonal regeneration both in vivo and in culture. *Invest Ophthalmol Vis Sci*. 2000;41:3943–3954.
20. Jiang G, Sun D, Yang H, Lu Q, Kaplan H, Shao H. HMGB1 is an early and critical mediator in an animal model of uveitis induced by IRBP-specific T cells. *J Leukoc Biol*. 2014;95:599–607.
21. Liljekvist-Soltica I, Olofsson J, Johansson K. Progenitor cell-derived factors enhance photoreceptor survival in rat retinal explants. *Brain Res*. 2008;1227:226–233.
22. Sahaboglu A, Tanimoto N, Bolz S, et al. Knockout of PARG110 confers resistance to cGMP-induced toxicity in mammalian photoreceptors. *Cell Death Dis*. 2014;5:5e1234.
23. Schnichels S, Blak M, Hurst J, et al. Establishment of a retinal hypoxia organ culture model. *Biol Open*. 2017;6:1056–1064.
24. Stutzki H, Leibig C, Andreadaki A, Fischer D, Zeck G. Inflammatory stimulation preserves physiological properties of retinal ganglion cells after optic nerve injury. *Front Cell Neurosci*. 2014;8:1–10.
25. Valdés J, Trachsel-Moncho L, Sahaboglu A, et al. Organotypic retinal explant cultures as in vitro alternative for diabetic retinopathy studies. *ALTEX*. 2016;33:459–464.
26. Zhang M, Marshall B, Atherton S. Murine cytomegalovirus infection and apoptosis in organotypic retinal cultures. *Invest Ophthalmol Vis Sci*. 2008;49:295–303.
27. El Zaoui I, Behar-Cohen F, Torriglia A. Glucocorticoids exert direct toxicity on microvasculature: analysis of cell death mechanisms. *Toxicol Sci*. 2015;143:441–453.
28. Mohlin C, Johansson K. Death of photoreceptors in organotypic retinal explant cultures: implication of rhodopsin accumulation and endoplasmic reticulum stress. *J Neurosci Methods*. 2011;197:56–64.
29. Paquet-Durand F, Sanges D, McCall J, et al. Photoreceptor rescue and toxicity induced by different calpain inhibitors. *J Neurochem*. 2010;115:930–940.
30. Peynshaert K, Devoldere J, Forster V, et al. Toward smart design of retinal drug carriers: a novel bovine retinal explant model to study the barrier role of the vitreoretinal interface. *Drug Deliv*. 2017;24:1384–1394.
31. Tao Y, Chen T, Liu B, et al. Visual signal pathway reorganization in the cacna1f mutant rat model. *Invest Ophthalmol Vis Sci*. 2013;54:1988–1997.
32. Tao Y, Chen T, Liu B, et al. The neurotoxic effects of N-methyl-N-nitrosourea on the electrophysiological property and visual signal transmission of rat's retina. *Toxicol Appl Pharmacol*. 2015;286:44–52.
33. Xin H, Yannazzo J, Duncan R, Gregg E, Singh M, Koulen P. A novel organotypic culture model of the postnatal mouse retina allows the study of glutamate-mediated excitotoxicity. *J Neurosci Methods*. 2007;159:35–42.
34. Cen L, Ng T, Liang J, et al. Human periodontal ligament-derived stem cells promote retinal ganglion cell survival and axon regeneration after optic nerve injury. *Stem Cells*. 2018;36:844–855.
35. Johnson T, DeKorver N, Levasseur V, et al. Identification of retinal ganglion cell neuroprotection conferred by platelet-derived growth factor through analysis of the mesenchymal stem cell secretome. *Brain*. 2014;137:503–519.
36. Falsig J, Aguzzi A. The prion organotypic slice culture assay—POSCA. *Nat Protoc*. 2008;3:555–362.
37. White A, Heller J, Leung J, Tassoni A, Martin K. Retinal ganglion cell neuroprotection by an angiotensin II blocker in an ex vivo retinal explant model. *J Renin Angiotensin Aldosterone Syst*. 2015;16:1193–1201.
38. Kustermann S, Schmid S, Biehlmaler O, Kohler K. Survival, excitability, and transfection of retinal neurons in an organotypic culture of mature zebrafish retina. *Cell Tissue Res*. 2008;332:195–209.
39. Dutescu RM, Skosyrski S, Kociok N, et al. Multifocal ERG recordings under visual control of the stimulated fundus in mice. *Invest Ophthalmol Vis Sci*. 2013;54:2582–2589.
40. Fujii M, Sunagawa GA, Kondo M, Takahashi M, Mandai M. Evaluation of micro electroretinograms recorded with multiple electrode array to assess focal retinal function. *Sci Rep*. 2016;6:30719.
41. Homma K, Osakada F, Hirami Y, Jin ZB, Mandai M, Takahashi M. Detection of localized retinal malfunction in retinal degeneration model using a multielectrode array system. *J Neurosci Res*. 2009;87:2175–2182.
42. Reinhard K, Tikidji-Hamburyan A, Seitter H, et al. Step-by-step instructions for retina recordings with perforated multi electrode arrays. *PLoS One*. 2014;9:e106148.
43. Quiroga R, Nadasdy Z, Ben-Shaul Y. Unsupervised spike detection and sorting with wavelets and superparamagnetic clustering. *Neural Comput*. 2004;16:1661–1687.
44. Meister M, Pine J, Baylor D. Multi-neuronal signals from the retina: acquisition and analysis. *J Neurosci Methods*. 1994;51:95–106.
45. Green DG, Kapousta-Bruneau NV. A dissection of the electroretinogram from the isolated rat retina with microelectrodes and drugs. *Vis Neurosci*. 1999;16:727–741.
46. Penn RD, Hagins WA. Signal transmission along retinal rods and the origin of the electroretinographic a-wave. *Nature*. 1969;223:201–204.
47. Nymark S, Heikkinen H, Haldin C, Conner K, Koskelainen A. Light responses and light adaptation in rat retinal rods at different temperatures. *J Physiol*. 2005;567:923–938.
48. Baden T, Berens P, Franke K, Rosón MR, Bethge M, Euler T. The functional diversity of retinal ganglion cells in the mouse. *Nature*. 2016;529:345–350.
49. Sanes J, Masland R. The types of retinal ganglion cells: current status and implications for neuronal classification. *Annu Rev Neurosci*. 2015;38:221–246.
50. Berson DM, Castrucci AM, Provencio I. Morphology and mosaics of melanopsin-expressing retinal ganglion cell types in mice. *J Comp Neurol*. 2010;518:2405–2422.

Investigative Ophthalmology & Visual Science

51. Bringmann A, Reichenbach A. Role of Müller cells in retinal degeneration. *Front Biosci*. 2001;6:72.
52. Garcia-Valenzuela E, Sharma S, Pina A. Multilayered retinal microglial response to optic nerve transection in rats. *Mol Vis*. 2005;11:225–231.
53. Geller S, Lewis G, Fisher S. FGFR1, signaling, and AP-1 expression following retinal detachment: reactive Müller and RPE cells. *Invest Ophthalmol Vis Sci*. 2001;42:1363–1369.
54. Lewis G, Sethi C, Carter K, Charteris D, Fisher S. Microglial cell activation following retinal detachment: a comparison between species. *Mol Vis*. 2005;11:491–500.
55. Lupien C, Brenner M, Guérin S, Salesse C. Expression of glial fibrillary acidic protein in primary cultures of human Müller cells. *Exp Eye Res*. 2004;79:423–429.
56. Hughes S, Rodgers J, Hickey D, Foster R, Peirson S, Hankins M. Characterisation of light responses in the retina of mice lacking principle components of rod, cone and melanopsin phototransduction signalling pathways. *Sci Rep*. 2016;6:1–11.
57. Ivanova E, Yee C, Baldoni R Jr, Sagdullaev B. Aberrant activity in retinal degeneration impairs central visual processing and relies on Cx36-containing gap junctions. *Exp Eye Res*. 2016; 150:81–89.
58. Orlans H, Edwards T, De Silva S, Patrício M, MacLaren R. Human retinal explant culture for ex vivo validation of AAV gene therapy. *Methods Mol Biol*. 2018;1715:289–303.
59. Osborne A, Hopes M, Wright P, Broadway D, Sanderson J. Human organotypic retinal cultures (HORCs) as a chronic experimental model for investigation of retinal ganglion cell degeneration. *Exp Eye Res*. 2016;14:28e38.
60. Pasha S, Münch R, Schäfer P, et al. Retinal cell death dependent reactive proliferative gliosis in the mouse retina. *Sci Rep*. 2017;7:1–16.
61. Rettinger C, Wang H. Quantitative assessment of retina explant viability in a porcine ex vivo neuroretina mode. *J Ocul Pharmacol Ther*. 2018;34:521–530.
62. Smedowski A, Pietrucha-Dutczak M, Maniar R, Ajeleti M, Matuszek I, Lewin-Kowalik J. FluoroGold-labeled organotypic retinal explant culture for neurotoxicity screening studies. *Oxid Med Cell Longev*. 2018;2487473:1–11.
63. Trifunović D, Petridou E, Comitato A, Marigo V, Ueffing M, Paquet-Durand F. Primary rod and cone degeneration is prevented by HDAC inhibition. *Adv Exp Med Biol*. 2018; 1074:367–373.
64. Vighi E, Trifunović D, Veiga-Crespo P, et al. Combination of cGMP analogue and drug delivery system provides functional protection in hereditary retinal degeneration. *Proc Natl Acad Sci U S A*. 2018;115:E3006.
65. Fisher S, Lewis G, Linbeg K, Verardo M. Cellular remodeling in mammalian retina: results from studies of experimental retinal detachment. *Prog Retin Eye Res*. 2005;24:395–431.
66. Löffler K, Schäfer P, Völkner M, Holdt T, Karl M. Age-dependent Müller glia neurogenic competence in the mouse retina. *Glia*. 2015;63:1809–1824.
67. Winkler J, Hagelstein S, Rohde M, Laqua H. Cellular and cytoskeletal dynamics within organ cultures of porcine neuroretina. *Exp Eye Res*. 2002;74:777–788.
68. Strauss O. The retinal pigment epithelium in visual function. *Physiol Rev*. 2005;85:845–881.
69. Bandyopadhyay M, Rohrer B. Photoreceptor structure and function is maintained in organotypic cultures of mouse retinas. *Mol Vis*. 2010;16:1178–1185.
70. Di Lauro S, Rodriguez-Crespo D, Gayoso MJ, et al. A novel coculture model of porcine central neuroretina explants and retinal pigment epithelium cells. *Mol Vis*. 2016;22:243–253.
71. Kaempf S, Walter P, Salz A, Thumann G. Novel organotypic culture model of adult mammalian neurosensory retina in co-culture with retinal pigment epithelium. *J Neurosci Methods*. 2008;173:47–58.
72. Kobuch K, Hermann W, Framme C, Sachs H, Gabel V, Hillenkamp J. Maintenance of adult porcine retinal pigment epithelium in perfusion culture: characterisation of an organotypic in vitro model. *Exp Eye Res*. 2008;86:661–668.
73. Rodriguez-Crespo D, Di Lauro S, Singh A, et al. Triple-layered mixed co-culture model of RPE cells with neuroretina for evaluating the neuroprotective effects of adipose-MSCs. *Cell Tissue Res*. 2014;358:705–716.
74. Berkelaar M, Clarke DB, Wang YC, Bray GM, Aguayo AJ. Axotomy results in delayed death and apoptosis of retinal ganglion cells in adult rats. *J Neurosci*. 1994;14:4368–4374.
75. Germain F, Calvo M, de la Villa P. Rabbit retinal ganglion cell survival after optic nerve section and its effect on the inner plexiform layer. *Exp Eye Res*. 2004;78:95–102.
76. Manabe S, Kashii S, Honda Y, Yamamoto R, Katsuki H, Akaike A. Quantification of axotomized ganglion cell death by explant culture of the rat retina. *Neurosci Lett*. 2002;334: 33–36.
77. Pérez De Sevilla Müller L, Shelley J, Weiler R. Displaced amacrine cells of the mouse retina. *J Comp Neurol*. 2007;505: 177–189.
78. Jeon CJ, Strettoi E, Masland RH. The major cell populations of the mouse retina. *J Neurosci*. 1998;18:8936–8946.
79. Segev R, Goodhouse J, Puchalla J, Berry MJ II. Recording spikes from a large fraction of the ganglion cells in a retinal patch. *Nat Neurosci*. 2014;7:1154–1161.
80. Borowska J, Trenholm S, Awatramani GB. An intrinsic neural oscillator in the degenerating mouse retina. *J Neurosci*. 2011; 31:5000–5012.
81. Goo Y, Park D, Ahn J, Senok S. Spontaneous oscillatory rhythms in the degenerating mouse retina modulate retinal ganglion cell responses to electrical stimulation. *Front Cell Neurosci*. 2016;9:1–8.
82. Margolis DJ. Functional stability of retinal ganglion cells after degeneration-induced changes in synaptic input. *J Neurosci*. 2008;28:6526–6536.
83. Stasheff S. Emergence of sustained hyperactivity and temporary preservation of OFF responses in ganglion cells of the retinal degeneration (rd1) mouse. *J Neurophysiol*. 2008;99: 1408–1421.
84. Berson DM, Dunn FA, Takao M. Phototransduction by retinal ganglion cells that set the circadian clock. *Science*. 2002;295: 1070–1073.
85. Hattar S, Liao H, Takao M, Berson D, Yau K. Melanopsin-containing retinal ganglion cells: architecture, projections, and intrinsic photosensitivity. *Science*. 2002;295:1065–1070.
86. Lucas R, Lall G, Allen A, Brown T. How rod, cone, and melanopsin photoreceptors come together to enlighten the mammalian circadian clock. *Prog Brain Res*. 2012;199:1–18.
87. Lin B, Koizumi A, Tanaka N, Panda S, Masland RH. Restoration of visual function in retinal degeneration mice by ectopic expression of melanopsin. *Proc Natl Acad Sci U S A*. 2008; 105:16009–16014.
88. Robinson GA, Madison RD. Axotomized mouse retinal ganglion cells containing melanopsin show enhanced survival, but not enhanced axon regrowth into a peripheral nerve graft. *Vision Res*. 2004;44:2667–2674.
89. Pérez de Sevilla Müller L, Sargoy A, Rodriguez A, Brecha N. Melanopsin ganglion cells are the most resistant retinal ganglion cell type to axonal injury in the rat retina. *PLoS One*. 2014;9:e93274.
90. Bringmann A, Iandiev I, Pannicke T, et al. Cellular signaling and factors involved in Müller cell gliosis: neuroprotective and detrimental effects. *Prog Retin Eye Res*. 2009;28:423–451.

Investigative Ophthalmology & Visual Science

91. Fernandéz-Sânchéz L, Lax P, Campello L, Pinilla I, Cuenca N. Astrocytes and Müller cell alterations during retinal degeneration in a transgenic rat model of retinitis pigmentosa. *Front Cell Neurosci*. 2015;9:1–16.

92. Hippert C, Graca A, Barber A, et al. Müller glia activation in response to inherited retinal degeneration is highly varied and disease-specific. *PLoS One*. 2015;10:e0120415.

93. Shen W, Fruttiger M, Zhu L, et al. Conditional Müller cell ablation causes independent neuronal and vascular pathologies in a novel transgenic model. *J Neurosci*. 2012;32:15715–15727.

94. Suga A, Sadamoto K, Fujii M, Mandai M, Takahashi M. Proliferation potential of Müller glia after retinal damage varies between mouse strains. *PLoS One*. 2014;9:e94556.

95. Nguyen J, Soto I, Kim K, et al. Myelination transition zone astrocytes are constitutively phagocytic and have synuclein dependent reactivity in glaucoma. *Proc Natl Acad Sci U S A*. 2011;108:1176–1181.

96. Jadhav A, Roesch K, Cepko C. Development and neurogenic potential of Müller glial cells in the vertebrate retina. *Prog Retin Eye Res*. 2009;28:249–262.

97. Karl M, Hayes S, Nelson B, Tan K, Buckingham B, Reh T. Stimulation of neural regeneration in the mouse retina. *Proc Natl Acad Sci U S A*. 2008;105:19508–19513.

Investigative Ophthalmology & Visual Science